TWO-DIMENSIONAL SELF-ASSEMBLIES OF

GOLD NANOPARTICLE-POLY(VINYL ALCOHOL) CONJUGATES

FROM AQUEOUS SOLUTION

Shelly Teng Teng Hsiao

A thesis presented to the faculty of Mount Holyoke College

in partial fulfillment of the requirements for the degree of

Bachelor of Arts with Honors

Department of Chemistry

South Hadley, Massachusetts

May 2010

This thesis was prepared under the

direction of Dr. Wei Chen

for 8 credits of independent study

For my mother, father, and brothers

ACKNOWLEDGEMENTS

To my research advisor, Wei Chen, for being my mentor, believer, and encourager through the long, yet enjoyable journey of this project. I have endured and crossed the finish line all because of your support.

To my mother, father, and brothers, for their unconditional love and strong upbringings, and for always believing in me and being proud of me no matter the outcome. I dedicate every one of my accomplishments to you all.

To Insun, Lan, Maria, Dana, Mojun, Alison, Mimi, and Genevieve. Thank you for all the laughter and food during group meetings and trips.

To Marian Rice, for mentoring me to operate TEM all on my own.

To Olivia Hsiao, my cousin and my telepathic twin. You are a great listener. I don't know where I would be without you today.

To Hannah Schmitz and Alexa Beyor, my two favorite artsy roomies. I appreciate all those late night talks about the present and the future.

To Isaac Halloran, no matter the distance, you are always there for me. Thank you. I'll always remember you telling me: "Don't Panic!"

To the BlasianPersuasians, the most diverse group of friends I had at MHC. Thank you for always keeping me sane, and entertained.

To all my dearest friends—STOCK, from MHC, Seattle, WA, and Brisbane, Australia—thank you for the fun memories and invaluable friendship.

TABLE OF CONTENTS

LIST OF FIGURES AND TABLES

Page Number

ABSTRACT

Controlled nanoparticle self-assembly is of great interest in attaining novel optical and electronic properties when incorporating nanomaterials in devices. This study examines self-assemblies of gold nanoparticle-poly (vinyl alcohol) (Au NP-PVOH) conjugates from aqueous solution. Au NPs are one of the most stable nanoparticles and they have wide applications in catalysis, biology, and cancer therapy. PVOH is a biocompatible polymer that helps to stabilize Au NPs from aggregating and it has film-forming capabilities. It is commercially available in various molecular weights and degrees of hydrolysis. Three 0.1% PVOH samples of comparable molecular weights and different extents of hydrolysis –13-23 kDa (98% hydrolysis), 13-23 kDa (88% hydrolysis), and 9-10 kDa (80% hydrolysis) – were adsorbed onto 15 nm Au NPs in aqueous solution. The Au NP-PVOH aqueous solutions were centrifuged and washed to concentrate conjugates and to remove excess PVOH chains, respectively. A drop was then casted on a UV-treated carbon-coated transmission electron microscopy (TEM) grid and annealed at 110 °C under nitrogen to promote uniform drying and two-dimensional (2D) self-assembly. 2D self-assemblies of Au NP-PVOH conjugates of all three types of PVOH were observed using TEM.

INTRODUCTION

Scientists have long been fascinated by metallic nanoparticles because of their colorful colloidal solutions before the introduction of nanotechnology and its applications in modern society.[1] Metal nanoparticles are renowned for their unique optical and electronic properties, which are different from those of bulk metals, due to quantum confinement effect and their large surface-area-to-volume ratio. In addition, the intrinsic properties are defined by size, shape, composition, crystallinity, and structure of metal nanoparticles.[2] Gold nanoparticles (Au NPs), in particular, have been extensively studied because they are one of the most stable metal nanoparticles and have wide applications in catalysis and biology.[3] Additionally, Au NPs possess other beneficial properties such as biocompatibility, bioinertness, and good interaction with biomolecules. Therefore, better understanding and control of properties of Au NPs can lead to new diagnostic applications in medicine and nanodevices.[2]

I. Gold nanoparticles

Au NP suspended in water or colloidal gold was used as early as the 4th or 5th century B.C. for aesthetic purposes to make ruby-stained glass and to color ceramics. A famous example of colloidal gold use is the Lycurgus Cup that is ruby red in transmitted light and green in reflected light. In the Middle Ages, soluble gold was even used to cure diseases such as heart problems, dysentery, epilepsy, tumors, and syphilis.[1, 3] In 1676, a German chemist

Johann Kunckels published a book about drinkable gold and its curative properties, and concluded "gold must be present in such a degree of communition that it is not visible to the human eye." Later in 1857, Michael Faraday proposed that the red color was due to gold in the colloidal form and he investigated the optical properties of thin films of dried gold colloidal solutions.[3]

Today, the physical properties of Au NPs, as those of other nanoparticles, are found to be size and shape dependent due to the coherent oscillation of the conduction band electrons (surface plasmon resonance). The surface plasmon resonance (SPR) is induced by their interaction with an electromagnetic field, which is responsible for Au NPs to absorb and scatter light stronger than other materials.[4] In 1908, a German physicist, Gustav Mie, first theoretically described the strong absorption band in the visible region and the scattering of electromagnetic radiation by spherical metal particles by solving Maxwell's equations.[1, 5] Surface plasmon absorption has been shown to be dependent on Au NP size and shape. For example, the maxima of the surface plasmon absorption for 9, 15, 22 nm spherical nanoparticles are 517, 520, and 521 nm,[1] respectively, which give Au NPs of different sizes varying hues of intense red color. When the shape is changed from spherical to rodlike, the plasmon absorption splits into two bands: transverse plasmon absorption and longitudinal plasmon absorption corresponding to oscillation of the free electrons perpendicular to and along the long axis of the rods,

respectively. The transverse plasmon absorption band at 520 nm is similar to that of spherical particles whereas the longitudinal band is red-shifted and depends on the nanorod aspect ratio, R, which is the length divided by the width of the rod.[6]

In order to control surface plasmon absorption, there are various methods of Au NP synthesis to exert control over size and shape of Au NPs. One popular method is called the citrate method, which uses trisodium citrate to reduce tetrachloroauric acid (HAuCl$_4$). Citrate acts as a reducing agent of HAuCl$_4$ and a stabilizer of Au NPs. The resulting Au NPs are coated with a layer of citrate (Figure 1).
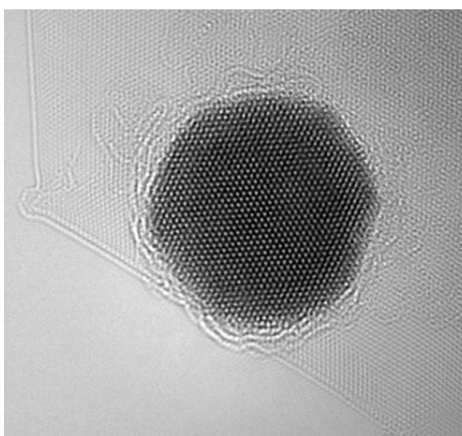
Figure 1: Transmission electron microscopy (TEM) image of a 10 nm citrate-coated Au NP.[7]

A proposed mechanism of Au NP formation by the citrate method suggests that the reaction occurs step-by-step, and notes that not all the steps

are well known today. The initial step of Au NP formation is the oxidation of citrate to yield dicarboxy acetone. Then the auric salt (Au^{3+}) gets reduced to aurous salt (Au^+) and the aurous species disproportionate into gold atoms. Dicarboxy acetone plays a big role in nucleation by acting as an organizer in forming a complex with the gold ions during the disproportionation step (Scheme 1, steps a–d).

Once the gold atoms are formed they adsorb Au^+ and further complex with dicarboxy acetone to form large aggregates. This step repeats until the aggregates reach a critical size, when the nucleus of gold atoms is formed. Depending on the ratio of the initial concentrations of citrate to $HAuCl_4$, varying sizes of monodisperse Au NPs can be synthesized.[8]

Scheme 1: Reduction mechanism of HAuCl$_4$ to Au^o by the citrate method. [8,9]

$$+ CO_2 + H^+ + 2e^- \qquad\text{(a)}$$

$$AuCl_3 + 2e^- \rightarrow AuCl + 2Cl^- \qquad\text{(b)}$$

$$3AuCl \rightarrow 2Au^o + AuCl_3 \qquad\text{(c)}$$

(d)
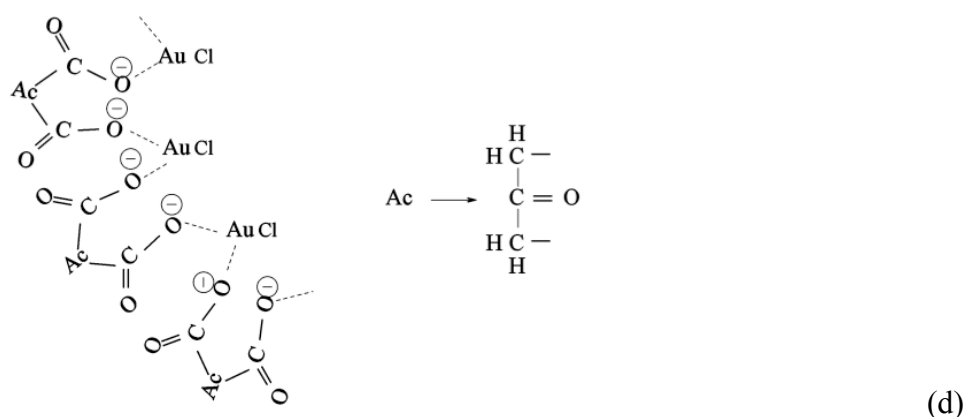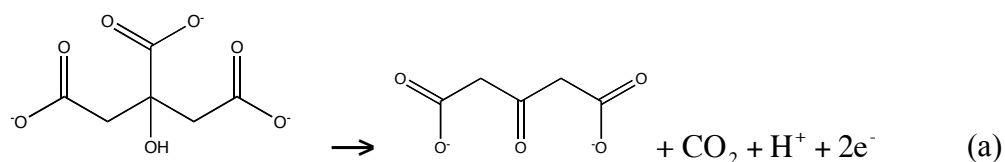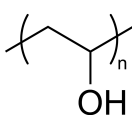
SPR is not only affected by the size and the shape of nanoparticles, but also by the presence of neighboring particles, hence SPR can be controlled by particle-particle interaction directed by interparticle spacing. In general, as neighboring particles are brought closer together, there is a red-shift in the SPR frequency due to the dipolar coupling of the particles.[10] Tamaru et al. reported, however, a strong anisotropy in the scattering spectra when different polarization directions were applied in the study of two neighboring spherical silver particles. Extending Tamaru et al.'s work, Rechberger et al. studied the surface plasmon extinction peaks of a range of interparticle distances between

two identical Au NPs. When the polarization direction of the incident light is parallel to the long particle pair axis, there is a red-shift of the SPR with decreasing interparticle distance. However, for the orthogonal polarization, there is a smaller, but distinct blue-shift of the peak.[11] Therefore, controlled and predictable interparticle spacing in ordered nanoparticle superlattices is necessary to seize optical properties for many applications.[10]

II. Poly(vinyl alcohol)

Stable and predictable assemblies of Au NPs are essential to ensure that their novel optical and electronic properties are attained in devices or applications. The stability and assembly of nanomaterials in solution is restricted by their Brownian motion, nanoparticle surface chemistry, and solution ionic strength (and pH). Brownian motion can lead to random collision and aggregation of NPs, which can result in uncontrollable and unpredictable nanomaterial properties.[12] Thus, to achieve a better stabilization or dispersion of metal NPs in aqueous media, various polymers have been used. The most commonly used polymers are poly(N-vinyl-2-pyrrolidone) (PVP),[13] polystyrene,[10] and poly(vinyl alcohol) (PVOH)[14, 15]. Polymers help to stabilize metal NPs by preventing aggregation through a steric stabilization mechanism.[16]

Poly(vinyl alcohol) (PVOH), OH , is an exceptional polymer

because it is nontoxic and has good water solubility, a high melting

temperature, and the ability to crystallize and form hydrogen bonds.[17]

Additionally, because PVOH is biocompatible, it is safe to use in

pharmaceutical and biomedical applications. PVOH is prepared by free radical

polymerization of vinyl acetate followed by hydrolysis.[18] The physical

properties of PVOH are dependent upon the molecular weight and the degree

of hydrolysis.

III. Self-assembly of Au NPs adsorbed with PVOH

The study of PVOH adsorption on citrate-coated Au NPs is an ongoing

study in Professor Wei Chen's lab (Figure 2).[19] This research takes advantage

of the understanding gained from PVOH adsorption studies on Au NPs and

focuses on preparing self-assembled two-dimensional hexagonal lattices of

Au NP-PVOH conjugates in solid state from aqueous solution (Figure 3). The

assemblies of uniform nanoparticles into two- and three-dimensional (2D and

3D) superlattices have been of great research interest in order to obtain novel

properties for potential applications in optical gratings, optical filters, data

storage, and microelectronic devices.[20] Additionally, the 2D and 3D

superlattices are important to chemical, optical, magnetic, and electronic

nanodevices.[21] Therefore, various techniques, such as self-assembly,

Langmuir-Blodgett (LB) techniques, and electrophoretic deposition method have been used to obtain 2D and 3D hexagonal superlattices.[22]

Self-assembly or spontaneous assembly of nanoparticles depends on hard sphere repulsion, steric repulsion of suface molecules, monodipersity of particle size, and van der Waals attraction between the particles. A limitation to creating 2D and 3D structures in solid state from an aqueous solution is the creation of circular voids that excludes nanoparticles once the solvent evaporates when the colloidal solutions are allowed to dry on substrates. Another challenge is that water soluable colloids aggregate once the solvent evaporates instead of forming ordered 2D and 3D structures. Therefore, previous studies have used organic solvents such as alkanes (e.g. hexane and heptane), toluene, and chloroform to avoid circular voids, and thiol-terminated molecules to bind to nanoparticle surfaces in order to prevent aggregation by controlling interparticle spacing.[20]
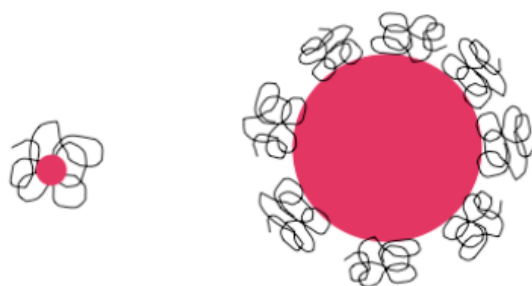
Figure 2: Configurations of adsorbed PVOH chains on two different sized Au NPs.

(a)
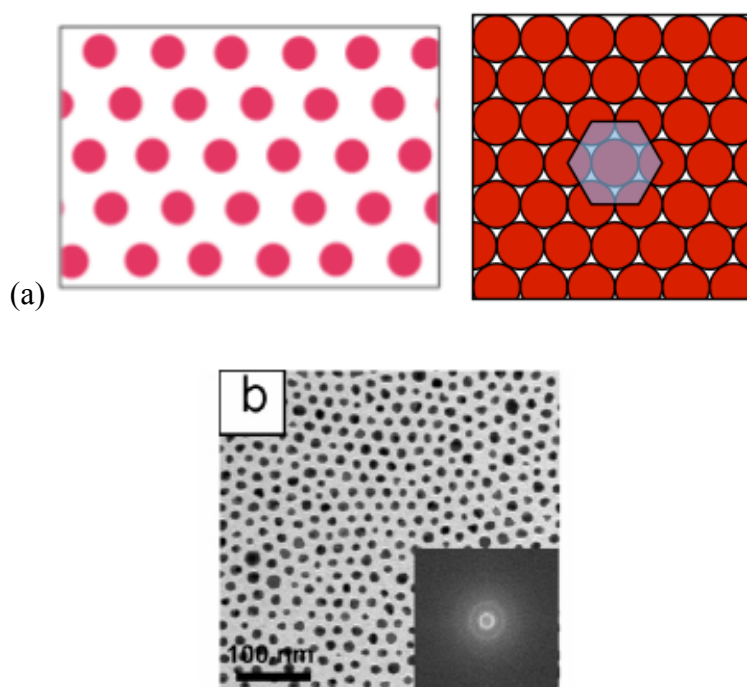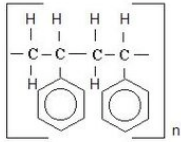
Figure 3: (a) Diagrams of two-dimensional hexagonal lattices of Au NP-PVOH conjugates with different interparticle spacing; and
(b) a TEM image of citrate reduced Au NPs with surface grafted polystyrene.[10]

Thiol-stabilized Au NPs[22] and dodecanethiol-stabilized silver (Ag) NPs[23] in toluene dispersions, and Ag NPs capped with 1-nonanethiol[24] and amine-stabilized Au NPs[25] in chloroform or dichloromethane have been reported in the literature to achieve 2D and 3D hexagonal superlattices. Furthermore, other methods of forming 2D and 3D superlattices include adding destabilizing molecules such as HCl or 4-pyridinecarboxylic acid, which changes the mercaptosuccinic acid (MSA) coated Au NPs from charged to neutral. The ordered 2D and 3D superlattices result from the loss of electrostatic repulsion among Au NPs.[20]

Zhao et. al. reported the first 2D assembly of Au NPs from stable hydrosol by using octanethiol-stabilized Au NPs in water and casting a drop on a carbon-coated copper TEM grid. Octanethiol was coordinated to the Au NP surface via the thiol group, which left a hydrocarbon tail exposed to water. Hydrophobic alkanethiol-stabilized Au NPs are not soluble in water,[26] therefore ethanol was first added to octanethiol aqueous solution before being combined with the Au NP solution. The Au NP self-assembly was found to be homogenous, highly ordered, and neither aggregates nor voids were seen in the monolayer.[22] Au NP aggregation was prevented since Au NPs were stabilized by both octanethiol and ethanol. This was the only report in the literature of ordered 2D self-assembly of Au NPs from aqueous solution, however, the addition of ethanol was found necessary.

The interspacing of self-organized Au NPs depends on the length or the molecular weight of the capping agent.[27, 28] Studies have shown that Au NPs adsorbed or covalently grafted with polymer chains such as polystyrene

(PS),   , resulted in hexagonally ordered monolayers when the particles were casted onto solid substrates (a carbon film or a glass slide) from a chloroform solution. However, only Au NPs grafted with PS chains shorter than 13 kDa displayed prominent hexagonal superlattices. [10] Poly(dimethylsiloxane) (PDMS) of varying molecular weights has also been grafted to Fe_2O_3 to control interparticle distance. The PDMS-modified Fe_2O_3 NPs in hexane were observed to spontaneously assemble into hexagonal patterns on solid substrates. Similar to the polystyrene-grafted Au NPs, when the molecular weight of PDMS was increased, the interparticle distance increased and the packing became less ordered.[29] Another method from the literature to systematically control the interparticle spacing is the use of poly(amidoamine) (PAMAM) dendrimers. Thiol-passivated Au NPs were converted to monodisperse mixed monolayer protected clusters (MMPC) using thermal ripening[30] and the Murray place exchange reaction. Then the MMPCs were modified with carboxylic acids. The driving force of self-assembly is noted to be the electrostatic interaction between the terminal amine groups of the dendrimer and the carboxylic acids on MMPC.[31]

PAMAM dendrimers with four different generations (G_0-G_4) that varied in branching and size were used to achieve controlled interparticing spacing (Figure 4).
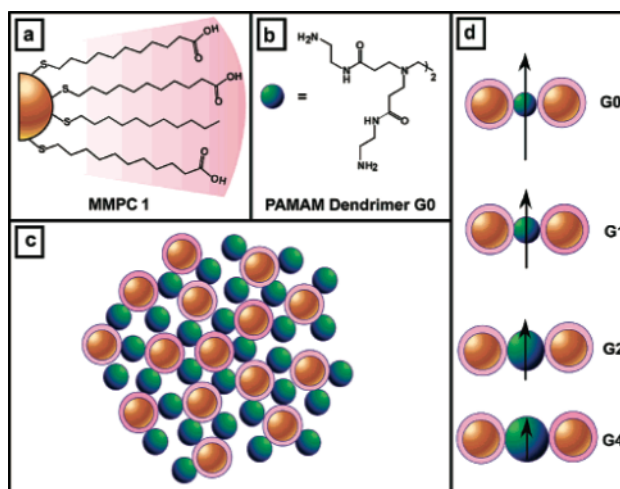
Figure 4: (a) MMPC with surface carboxylic acids; (b) structure of PAMAM dendrimer G_0; (c) self-assembled packing of MMPC with PAMAM dendrimers; (d) spacing between MMPCs due to various generations of PAMAM dendrimers.[31]

In order to avoid using linkers and destabilizing molecules, and to achieve concentrated Au NP solutions, Roca et al. assembled linear clusters of Au NPs by using citrate-stabilized Au NPs encapsulated in silica shells that were preconcentrated via high force centrifugation (9400 *g*). They found that, without centrifugation, Au NPs with silica coating formed a monolayer of individual Au NPs. However, when the silica coated Au NPs were centrifuged, both single and clusters of Au NPs were observed. This indicated that the formation of Au NP clusters, hence poorly ordered Au NP self-

assembly was attributed to centrifugation. Previous studies have shown that centrifugation can induce a polarization of the electrical double layer on the colloid surface[32] since the "lighter" ions remain stationary relative to the downward movement of the particle. Therefore, as a consequence of centrifugation, the polarized particles are forced downward in the tube, which leads to a decreased distance between the NPs, thus their electrical double layers overlap, leading to NP aggregations (Scheme 2).[12]

Scheme 2: (1) Electrical Polarization of Au NPs, and (2) Au NP assembly due to centrifugation, where the (3) Au NPs are encapsulated in silica.[12]
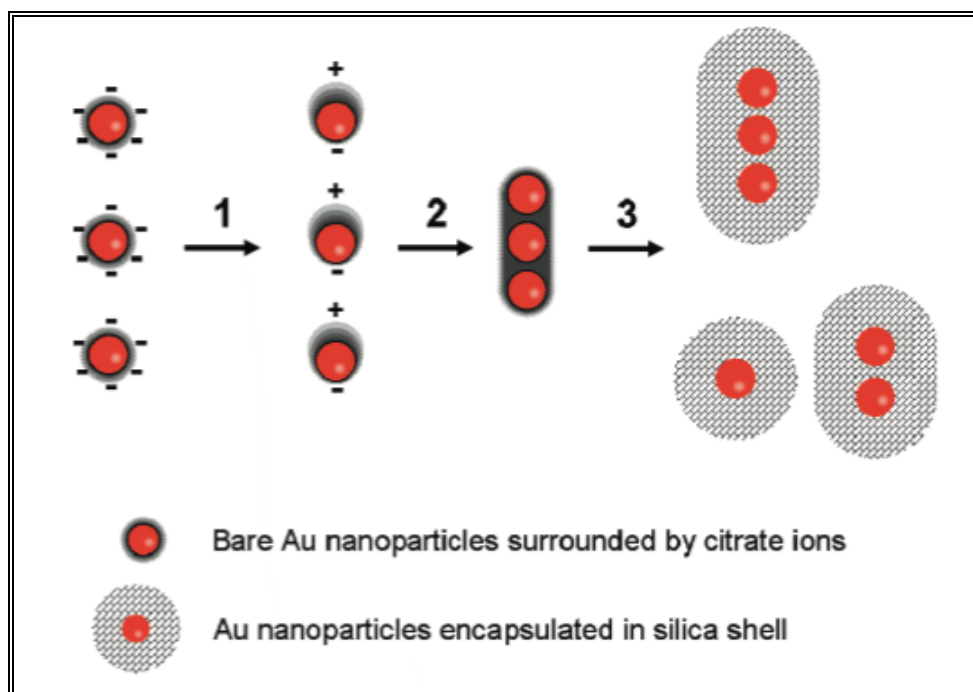
The aims of this research project are three folds. (1) Using 13-23 kDa and 98% hydrolyzed PVOH, and 15 nm Au NPs, determine the optimal concentration of Au NP-PVOH conjugates that promotes 2D self-assemblies. (2) Pick an optimal Au NP-PVOH concentration and introduce heat treatment to eliminate phase segregation and voids due to slow evaporation of water and to promote PVOH chain mobility for improved 2D self-assemblies. (3) Extend the study to incorporate two other PVOH solutions with comparable molecular weights, but different degrees of hydrolysis to examine if the variation in degree of hydrolysis of PVOH would elicit better 2D Au NP-PVOH self-assemblies.

INSTRUMENTAL METHODS

I. Transmission Electron Microscopy[33]

In this study, transmission electron microscopy (TEM) was utilized to examine the self-assemblies of Au NP-PVOH conjugates. TEM operates similarly to the basic principles of a light microscope except that TEM uses electrons instead of photons in order to achieve better resolution power. Also, TEM uses electromagnetic lenses instead of glass lenses since electrons are small particles that would get scattered by any surrounding media. TEM is operated under a vacuum system for four main reasons: first, electron's mean free path is increased since there isn't any collision with gas molecules; second, vacuum prevents high voltage discharges; third, it prevents oxidation of the filament, which is the source of electrons; fourth, it removes contaminating gases (water vapor and organics) that may get broken down into radicals under high-energy electron bombardment and react with the specimen. Collectively, TEM is able to achieve better resolution and higher magnification than light microscopy as shown in Figure 5.
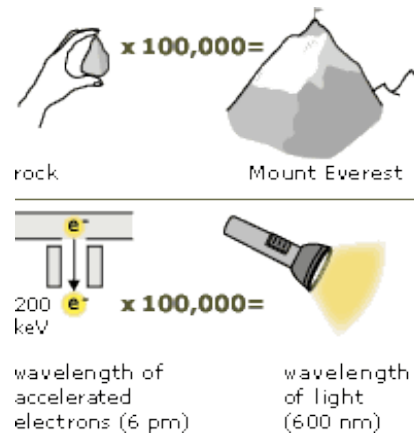
Figure 5: The wavelength of light from light microscopy is about 100,000 times greater than the wavelength of electrons from TEM.[33]

i. Resolution

Wavelength of visible light limits the resolution of light microscopy to around 0.172 μm using the resolving power equation:

$$r = \frac{0.612\lambda}{n(\sin\alpha)} \qquad (1)$$

where λ is the wavelength of illumination, n is the refractive index of the lens, and α is the aperture angle of the lens.

Better resolution can be achieved if a "light" source has a shorter wavelength than visible light according to equation (1). In fact, electrons, which have both particle and wave properties, were discovered to have much shorter wavelength than visible light. The wavelength (λ) of an electron can be expressed by the de Broglie's equation:

$$\lambda = \frac{h}{mv} \tag{2}$$

where h is Planck's constant, 6.626 X 10^{-34} Js, m is the electron mass, and v is electron velocity. The relationship between particle speed and voltage is:

$$qV = \frac{1}{2}mv^2 \tag{3}$$

where q is the charge of an electron and V is the voltage. Rearranging equation (3) to solve for speed, v, and substituting the equation for v into equation (2) gives:

$$\lambda = \frac{h}{\sqrt{2qVm}} \tag{4}$$

Substituting for mass of electrons (m = 9.1 x 10^{-31} kg), charge (q = 1.6 x 10^{-19} coulombs), and Planck's constant, the following equation of wavelength as a function of voltage is obtained:

$$\lambda = \frac{1.23}{\sqrt{V}} \text{ nm} \tag{5}$$

Therefore, if voltage (V) is set at 60 kV, the wavelength of the electron would be 0.005 nm, which would yield a resolution power of 0.003 nm. However, the actual resolution is about 0.1 nm due to limiting factors such as spherical aberration, chromatic aberration, and astigmatism. However, using electrons as a "light" source and their shorter wavelength, TEM is able to resolve objects thousands of times better than with a light microscope.[34]

ii. Magnification

Magnification (mag) is referred to the degree of enlargement of the final image to the original image:

$$\text{Mag} = \frac{\text{image distance}}{\text{object distance}} \tag{6}$$

In TEM, magnification is determined by at least three magnifying lenses: objective, intermediate, and project lenses. Therefore, the final magnification is the product of the individual magnifying powers:

$$M_T = M_o \text{ x } M_I \text{ x } M_P \tag{7}$$

where M_T is the total mag, M_o is the mag of objective lens, M_I is the mag of intermediate lens, and M_P is the mag of projector lens.

iii. A Guide of Electrons through a Transmission Electron Microscope

TEM consists of at least four systems that function to image extremely thin samples (Figure 6). Electrons are first emitted from a tungsten filament inside an electron gun at the top of the microscope column. Two condenser lenses gather and focus the electrons onto a sample. The first condenser (C1) decreases the size of the first crossover from the gun and the second condenser (C2) enlarges the C1 spot to generate a spot that illuminates the sample area (Figure 7).

(a)

(b)
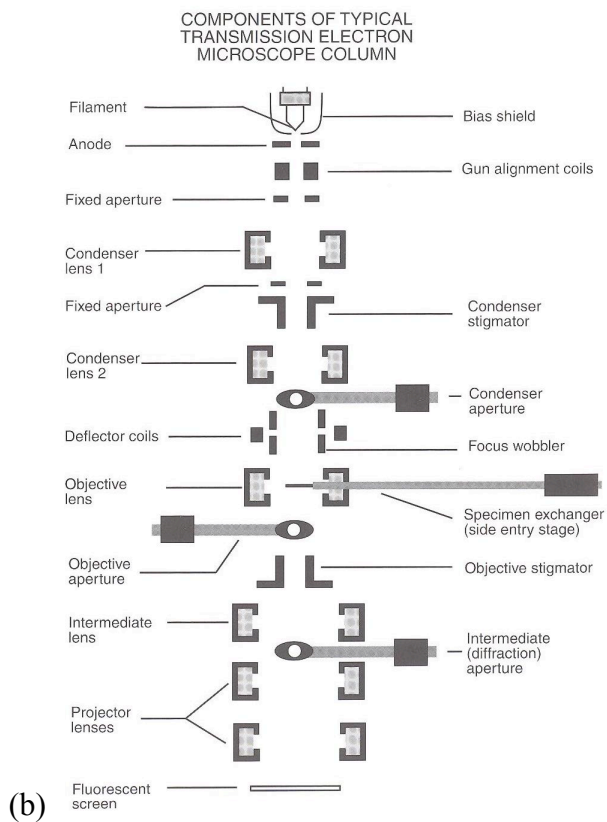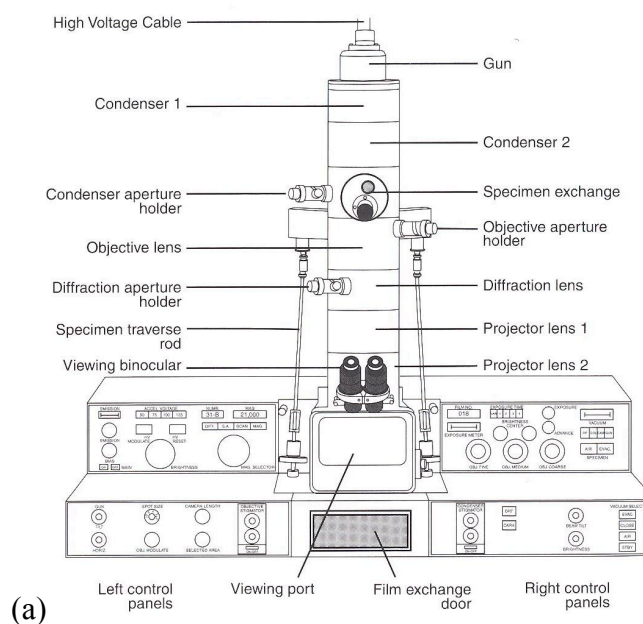
Figure 6: Overview of (a) exterior and (b) interior of a TEM with major components labeled.[33]
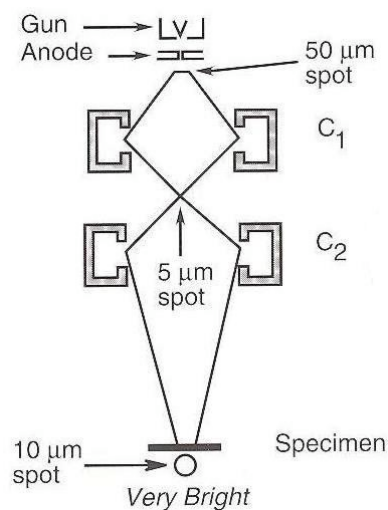
Figure 7: The condenser lens system (C_1 and C_2). Example: a 50 μm spot from the gun crossover is reduced to 5 μm by C_1 and then enlarged to 10 μm by C_2.[33]

The electrons then arrive at a set of electromagnetic lenses—objective, intermediate, and projector—that are involved in the magnification, generation, and projection of images that can be viewed on the viewing port or camera. The electrons from the condenser lens and through the sample get focused and magnified to form an initial image by the objective lens. In order to enhance image contrast, the objective aperture removes peripherally deflected electrons by decreasing the size of the aperture as shown in Figure 8. The intermediate lenses are responsible for magnifying the image from the objective lens. Sometimes they are used in place of the objective lens to achieve low magnifications. The projector lenses (P1 and P2 in Figure 6b) then further magnify images from the intermediate lens. The final image of the sample is projected onto a viewing screen. In our study, images of the two

dimensional self-assemblies of Au NP-PVOH conjugates can be transferred onto a film or taken by a digital camera and displayed on a computer screen.
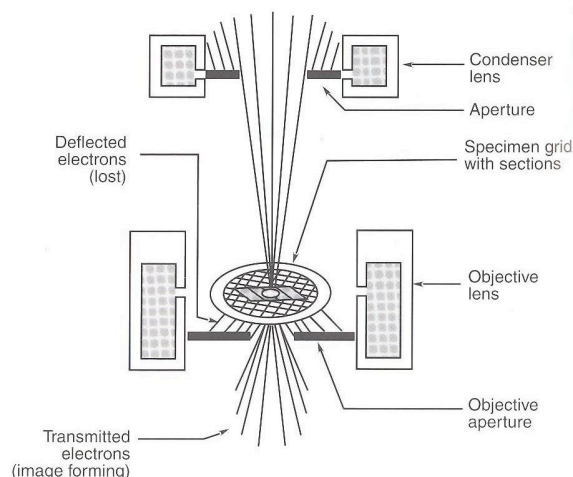
Figure 8: The objective lens primarily focuses and magnifies the image. The objective aperture enhances contrast by blocking deflected electrons.[33]

II. Dynamic Light Scattering[35,36]

Dynamic light scattering (DLS) was used to determine the size and monodispersity of Au NPs, poly(vinyl alcohol) chains, and Au NP-PVOH conjugates. DLS measures the Brownian motion of particles suspended in solution in order to calculate their size. Particles' translational motion in a dilute solution is due to the bombardment by surrounding solvent molecules. Smaller particles are correlated with faster Brownian motion because they move further and more rapidly after bombardment due to their small size.

The velocity of the Brownian motion is found by measuring the rate of intensity fluctuation of the scattered light by the particles in solution

(Figure 9). The fluctuation arises from the constantly evolving wave patterns from moving particles. Thus, the rate of intensity fluctuation depends on particle size (Figure 10a). The intensity measurements are taken at increasing time or correlation time. The correlation time starting at time = t increases by small increments of δt so that the intensity of a signal from time = t is compared to that at t + δt in order to construct a graph (Figure 10b).
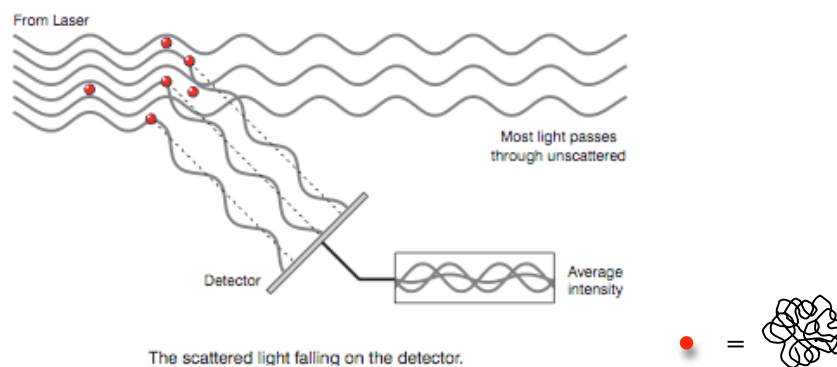
Figure 9: Schematic representation of the scattering of light by PVOH in a dynamic light scattering experiment.[35] Each dot represents a coiled PVOH chain.
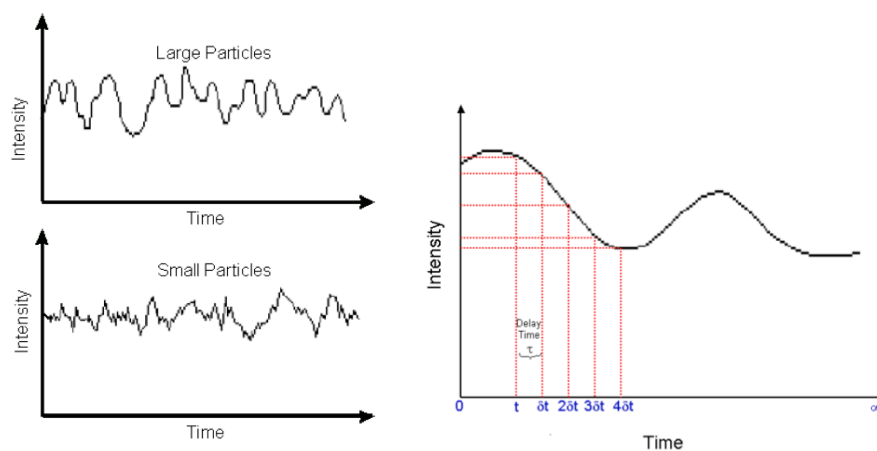
Figure 10: (Left) Intensity fluctuation for large and small particles. (Right) Schematic representation of the fluctuation in the intensity of scattered light as a function of time.[36]

The relationship between the intensity of the scattered light by particles and correlation time can be described as a correlation function, $G(\tau)$:

$$G(\tau) = \lim_{T \to \infty} \left[\frac{1}{T} \int_0^T i_\theta(t) i_\theta(t + \tau) dt \right] \tag{6}$$

where i_θ is the intensity of scattered light at angle θ, t is the sampling time, and τ is the correlation time.

Normalization of the correlation function yields a decay curve, $g(\tau)$:

$$g(\tau) = e^{-\Gamma \tau} \tag{7}$$

where the characteristic decay rate, Γ, is related to the translational diffusion coefficient, D:

$$\Gamma = \left(\frac{4\pi n \sin \frac{\theta}{2}}{\lambda} \right)^2 D \tag{8}$$

where D is the translational diffusion coefficient, n is the refractive index of the solvent, λ is the wavelength of the laser, and θ is the scattering angle. Thus, the diffusion coefficient, D, can be calculated by fitting the experimental data to an exponential curve and using equations (7) and (8).

Using the diffusion coefficient, which describes the rate of particle movement, the size of the particles can be determined (Figure 11). Assuming that the poly(vinyl alcohol) chains are random coils that are spherical in

shape, the relationship between the diffusion coefficient and the particle size

can be described by the Stokes-Einstein equation:

$$D_H = \frac{kT}{3\pi\eta D} \tag{9}$$

where D_H is the hydrodynamic diameter or particle size in solution, k is

Boltzmann's constant, η is the solution viscosity, and T is the absolute

temperature of the system.
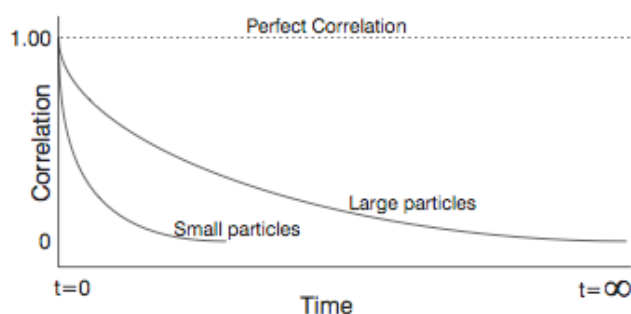
Figure 11: The characteristic decay rate can be used to determine particle size. The correlation of a signal of large particles take a longer time to decay than that of small particles as they continue to scatter light at increasing correlation time.[35]

In this study, DLS was used to measure the sizes of Au NPs, PVOH

chains, and Au NP-PVOH conjugates and to determine whether the dissolved

PVOH in aqueous solution were present as individual chains or aggregates

before being used to adsorb onto Au NPs. Monodisperse single PVOH chains

are desired in obtaining 2D self-assemblies of Au NP-PVOH conjugates since

aggregates of PVOH can interfere with ordered packing.[2-4]

EXPERIMENTAL

Poly(vinyl alcohol) preparation. 0.1 wt% of PVOH solution was prepared by Lanhe Zhang by dissolving PVOH powder (M_w = 13-23 kDa and 98% hydrolyzed, M_w = 13-23 kDa and 88% hydrolyzed, and M_w = 9-10 kDa and 80% hydrolyzed; Aldrich) in Milli-Q water (Millipore Milli-Q Biocel System, resistivity ≥ 18.2 MΩ/cm). Dissolution was performed in a hot water bath at 95°C for three hours or prepared at room temperature under stirring. The heated PVOH solution was cooled to room temperature (25°C) overnight under stirring. Before use, prepared PVOH solutions were filtered using 0.2 μm Nylon filter (Fisherbrand) to remove dust and PVOH aggregates.

Au NP Synthesis by the citrate method[9]. Using the citrate method, 50 mL of 0.25 mM HAuCl₄ (FW 393.83 kDa, 99+% hydrogen tetrachloroaurate (III) trihydrate; Aldrich) solution was heated to boil in a sand bath. Upon boiling, either 400μL, 625 μL, 875μL, or 2 mL of 3.4 x 10^{-2} M 1 wt% trisodium citrate (Fisher Science Company) was added to the boiling HAuCl₄ solution. Depending on the size of the Au NPs formed, which was controlled by the amount of citrate added, the final color of the gold solution varied from purplish red to deep red. The solution was kept to sit in the sand bath until the color of the solution stabilized and it was cooled to room temperature.

Dynamic light scattering (DLS) studies. In order to determine the size distribution of synthesized Au NPs and PVOH chains (before and after filtration), analyses were performed using a Malvern Zetasizer Nano-S instrument, equipped with a 4 mW He-Ne laser (λ = 633 nm). The refractive indices of PVOH, n = 1.520, and water at 25°C, n = 1.330, and the viscosity of water at 25°C, η = 0.8872 cP, were assigned to calculate the dimensions of Au NPs and PVOH chains. Samples were placed in low volume disposable polystyrene cuvettes (Fisher). Occasionally, dust contamination on the cuvettes and/or in the sample appeared as small peak(s) exceeding 1 μm in diameter on the size distribution plot based on scattering intensity. Experiments proceeded if the same peak(s) were absence in the size distribution plot based on scattering volume.

UV-treatment of TEM grids. Carbon-coated TEM grids (200 square mesh, Electron Microscopy Sciences) were hydrophilized to allow the even spreading of aqueous solutions. The grids were irradiated by a UV lamp (Model UVG-11, short wavelength UV-254 nm, 115 Volts 60Hz 0.16 Amps) that is 1 inch above for 30 minutes. Samples were casted immediately on the treated grids.

Concentrating Au NP-PVOH conjugates in solution for TEM

observation. 1: 4 volume ratio of 15 nm (synthesized in lab) or 15 nm

(commercially available from BBInternational) Au NP solution and 0.1 wt%

filtered PVOH were mixed and allowed to sit overnight to permit the

adsorption of PVOH chains onto Au NPs. 1.5 mL aliquots of Au NP-PVOH

solution were centrifuged (Eppendorf 5415 Microcentrifuge) for 30 minutes at

13,200 rpm (16,100 g force). A dense Au NP-PVOH pellet was formed after

the first round of centrifugation. Approximately 1.0 mL of the supernatant

was discarded before 1.5 mL of water was added to the centrifuge tube to

resuspend the Au NP-PVOH pellet. Three more rounds of centrifugation were

performed as described above in order to remove excess free PVOH chains

from the aqueous solution. After the last round of centrifugation and

decantation of supernatant, the amount of water added to resuspend the pellet

was chosen based on the desired final concentration. A small drop of the

concentrated Au NP-PVOH mixture was cast on a UV-treated TEM grid.

Some of the cast samples were dried at 110 °C under nitrogen for one hour.

The thin films on the TEM grids were then imaged using Philips CM 100

TEM operated at 80 kV. The images were taken using Kodak Megaplus

Camera, Model 1.6i.

RESULTS AND DISCUSSION

I. Au NP Synthesis. Monodisperse 15 nm, 16 nm, 46 nm, and 57 nm Au NPs were prepared using the citrate method by varying the amount of reducing agent, trisodium citrate (see Table 1, adjusted TEM size). As shown in Figure 12, there is an inverse correlation between the amount of citrate used and the Au NP size. As the amount of citrate is increased, more citrate molecules are available to reduce, organize, and form nucleation sites for Au^o to grow into Au NPs, and the Au NP size should decrease. Seconds after adding citrate to the boiling yellow $HAuCl_4$ solution, the solution color changed to blue indicating the formation of gold (Au^o) nuclei. Then after a minute or so, the solution changed to brownish purple, then lastly to a hue of red. The red color is an indication of Au NP formation[8] due to growth of nuclei into larger particles.

The 46 nm and 57 nm Au NPs are oval in shape whereas the 15 nm and 16 nm Au NPs are more spherical as seen in the TEM images of Figure 14. Typically, the larger Au NPs were purplish red in solution while the smaller particles were deep red due to the size dependence of SPR of Au NPs. The TEM images in Figure 14 display Au NPs clustered into aggregates, which is because without a capping agent, such as PVOH, citrate coated Au NPs tend to aggregate in solution due to random collision (Brownian motion) and Van der Waals attraction. Also, the high mechanical force during

centrifugation may result in aggregates due to induced polarization of the electrical double layer on the Au NP surface as discussed in the introduction section.[32]

The hydrodynamic (D_H) diameters of the four synthesized Au NP sizes were also measured using dynamic light scattering. The size distribution graph of 15 nm Au NPs is displayed in Figure 13 and the DLS sizes are reported in Table 1. The D_H values of Au NPs are slightly larger than the adjusted TEM values. The difference is attributed to the two methods of characterizing the size of the Au NPs. DLS measures the hydrodynamic size of Au NPs coated with a layer of citrate, whereas the TEM images only the electron dense Au NPs, excluding the citrate layer. Thus, the DLS measurements are an overestimate of the TEM measurements, but the trends of Au NP size are similar using the two methods.

UV-Vis absorption peaks near the 520 nm region for all four types of Au NPs confirmed that the Au NPs were spherical as previously reported by Link et al.[1] Slight variations in the peak position correspond to Au NPs of varying sizes.
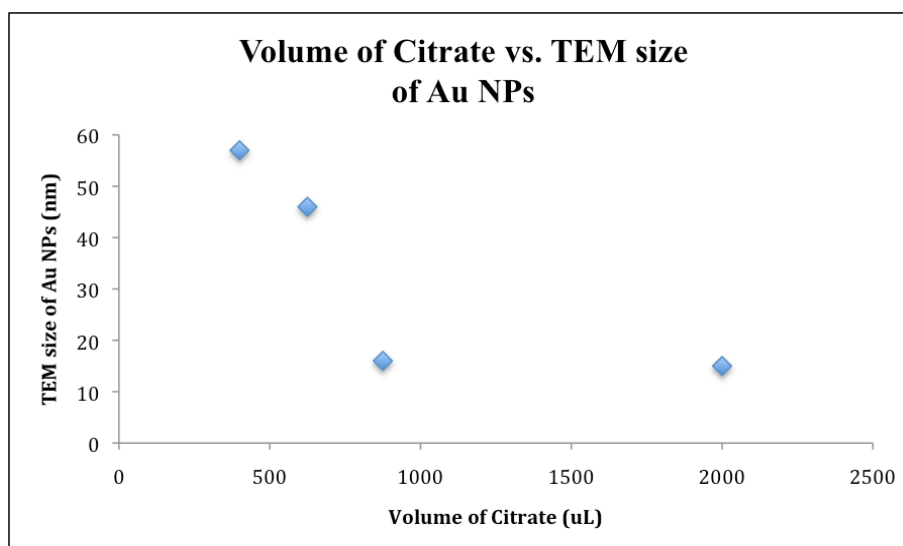
Figure 12: Au NP size is inversely related to the amount (varying volume used) of citrate.
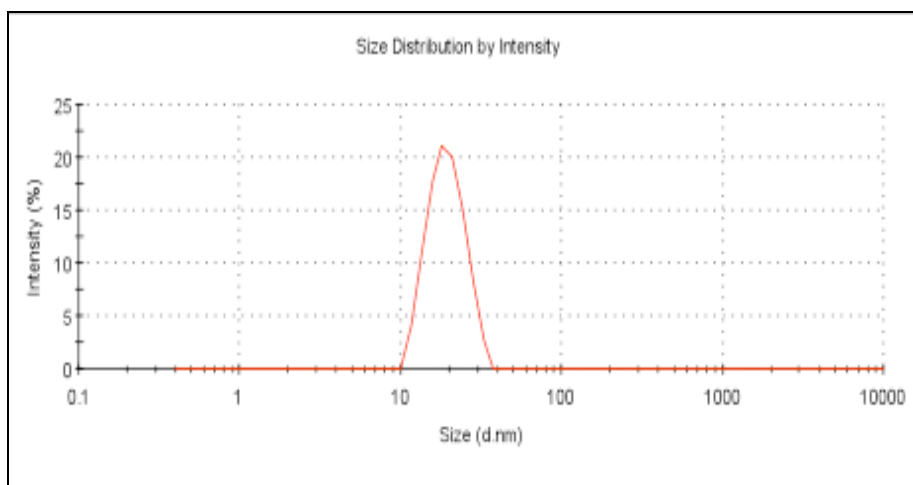
Figure 13: DLS intensity distribution of 15 nm Au NPs.
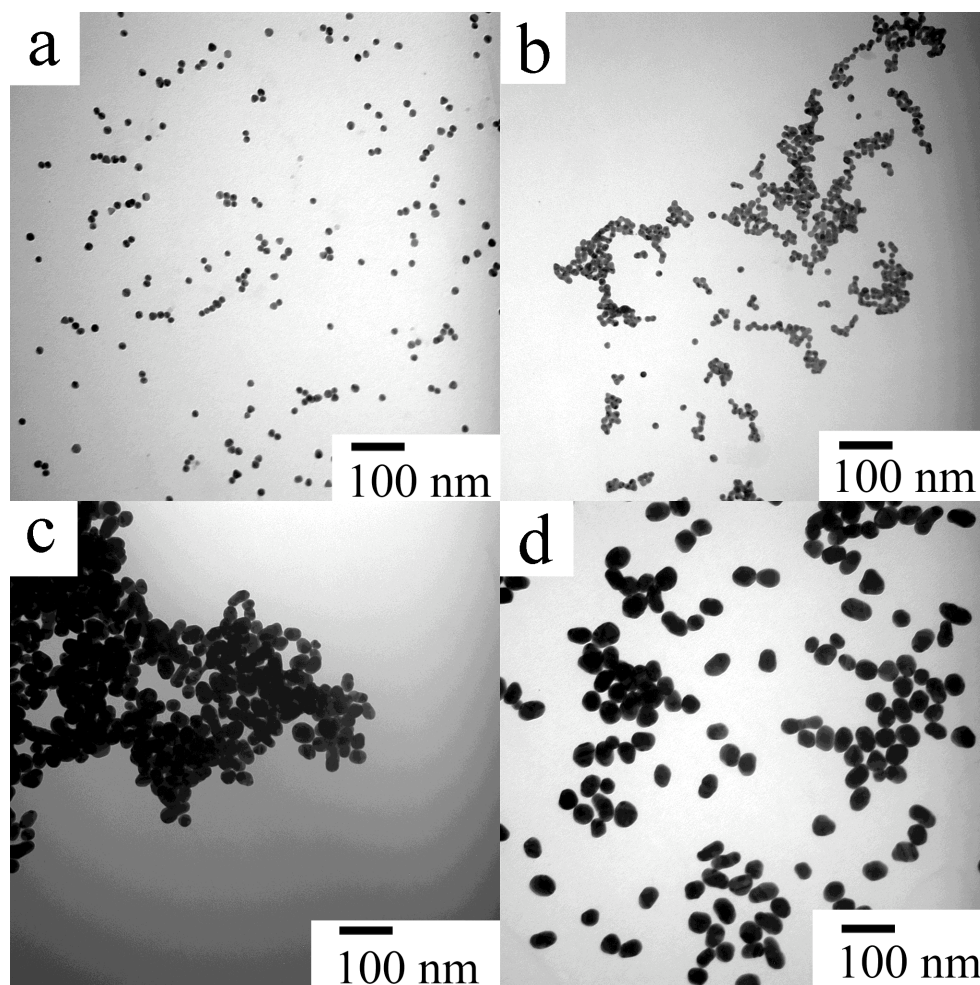
Figure 14: TEM images of Au NPs synthesized by the citrate method. (a-d) 15, 16, 46, 57 nm Au NPs (made from 50 mL of $HAuCl_4$ and 2 mL, 875μL, 625μL, 400μL of 3.4 x 10^{-2} M trisodium citrate, respectively).

Table 1: Size and color characterization of different Au NP sizes prepared by the citrate method.

Volume of 3.4 x 10^{-2} M 1wt% citrate (μL)	Raw TEM size (nm)	Adjusted[a] TEM size (nm)	D_H (nm)	UV-vis (nm)	Color
400 μL	40.9+/- 6.9	57	51.6 (87.1%) 4.6 (12.9%)	535	Purplish red
625 μL	32.9+/-6.6	46	49.4 (71.7%) 4.6 (28.3%)	531	Purplish red
875 μL	11.2+/-1.8	16	19.7 (100%)	520	Red
2 mL	10.7+/-2.1	15	20.9 (100%)	520	Deep red

[a] Actual size of Au NPs after TEM calibration. These sizes are used in the rest of the thesis.

II. Adsorption of PVOH onto 15 nm Au NPs. Yockell-Lelièvre et al.[10] reported 2D hexagonal self-assemblies of Au NPs conjugated to polystyrene (PS) when the PS chains were 13 kDa or shorter. The lowest molecular weights of PVOH that are commercially available are 9-10 kDa (80% hydrolysis), 13-23 kDa (88% hydrolysis), and 13-23 kDa (98% hydrolysis). This research focuses on these PVOH samples of similar molecular weights with varying degrees of hydrolysis. Excess free, single PVOH chains were adsorbed onto 15 nm Au NPs from aqueous solution during a 24-hour equilibration period at room temperature to form Au NP-

PVOH conjugates. Prior to adsorption, PVOH solutions were filtered to ensure the removal of PVOH aggregates, dust, and any other contaminants. The size distribution of PVOH chains in solution before and after filtration was determined using DLS. The hydrodynamic diameter (D_H) of PVOH chains after filtration was generally larger than that before filtration. This discrepancy could be due to the fact that the PVOH chains got stretched out when they were pushed through the pores of the filter. We hypothesize that, given sufficient time, the PVOH chains would relax back to their native conformations before they were adsorbed onto the Au NPs.

The size distribution of Au NP-PVOH conjugates ($D_{H,\ conjugates}$) and Au NPs with a layer of citrate ($D_{H,\ Au\ NPs}$) alone were also measured as shown in Table 2. The difference between the $D_{H,\ conjugates}$ and $D_{H,\ Au\ NPs}$ divided by two determines the thickness of PVOH adsorbed to the Au NP surface ($D_{H,\ PVOH\ thickness}$). The adsorbed PVOH thickness for 98%, 88%, and 80% degree of hydrolysis were 9.21 nm, 11.28 nm, and 8.64 nm, respectively. All three PVOH sizes were comparable to the average D_H of unfiltered free PVOH chains, which was 9.99 ± 0.90 nm. We can thus hypothesize that in aqueous solution, the conformation of the adsorbed PVOH chains is similar to that of free PVOH chains.

Table 2: DLS size measurement of PVOH thickness of varying degrees of hydrolysis.

Degrees of Hydrolysis	$D_{H, conjugates}$ (nm)	$D_{H, Au NPs}$ (nm)	$D_{H, PVOH thickness}$ (nm)
98%	40.18	21.36	9.41
88%	43.93	21.36	11.28
80%	38.03	21.36	8.64

III. Optimization of Au NP-PVOH conjugate concentration. Three factors affecting 2D self-assembly of Au NP-PVOH conjugates from aqueous solution were studied in this research. The first factor is Au NP-PVOH concentration. Various concentrations were prepared to find the optimal concentration that resulted in close packing of Au NPs to promote 2D self-assembly. To optimize the concentration of Au NP-PVOH conjugates, 13-23 kDa PVOH with the highest degree of hydrolysis (98%) was chosen for initial studies due to its known behavior and stability from previous studies in Professor Wei Chen's lab.[19] As stated above, Au NP-PVOH conjugates were first prepared. The Au NP-PVOH conjugates were then centrifuged and washed with water to concentrate and remove excess PVOH chains from the solution, respectively. The final concentrated Au NP-PVOH pellet was resuspended in water to the desired final volume, thus concentration. Finally a drop of the Au NP-PVOH conjugate solution was casted on a UV-treated carbon-coated TEM grid. Carbon-coated TEM grids were first hydrophilized by oxidizing the hydrophobic C=C to hydrophilic carboxyl, carbonyl, alcohol,

and other hydrophilic oxygen containing groups in order to promote uniform spreading of the Au NP-PVOH solution. The drop was allowed to air-dry on the grid at room temperature overnight. Once water evaporated, leaving behind a thin Au NP-PVOH film on top of the TEM grid, self-assembly was observed using a TEM.

For our initial study, 4 μL of the Au NP-PVOH solutions in 6x, 24x, 42x, 100x, and 200x of the initial concentration was cast on TEM grids. At 6x, 24x, and 42x (Figure 16), the Au NPs were sparse and there weren't enough Au NPs present to promote 2D self-assembly. Thus, the concentration was increased to 100x and 200x. At both 100x and 200x, the increase in Au NPs promoted localized regions of 2D self-assemblies. However, at 200x, there were 3D self-assemblies where the Au NPs were overlapping one another as indicated by the darker regions. Au NP aggregation may have resulted in 3D self-assembly and a loss of 2D self-assembly. More likely however, the aggregation could be due to an overwhelming number of Au NPs on the TEM grid and the coffee ring effect. In order to understand how the Au NP-PVOH solution dries on the hydrophilic TEM grid, we can first study how a drop of coffee dries since the drying process doesn't depend on solute.[37] Upon drying, a dark band lines the perimeter of the drop indicating that most of the coffee residues deposit at the edge. The mechanism of the coffee ring effect can be explained by capillary flow, i.e. the liquid evaporating from the edge must be replenished by the liquid in the interior as illustrated in Figure 15. Relating the

coffee ring effect to the drying process of a drop of Au NP-PVOH, more Au

NPs deposited near the edge of the drop, leaving particle poor region in the

center and particle rich region near the edge of the grid. Thus, the Au NP

distribution throughout the grid was heterogeneous, and as a consequence, in

the regions where close packing occurred, there were Au NP-PVOH

aggregates contributing to 3D self-assembly instead of 2D self-assembly.
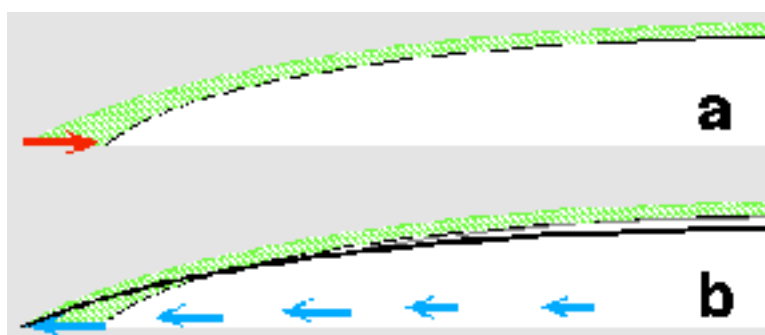
Figure 15: Schematic mechanism of the coffee ring effect due to capillary flow: (a) a cross-section of a drop, where the shaded region represents the volume of liquid that evaporated after an infinitesimal increment of evaporation; (b) the liquid evaporated from the edge must be replenished by the liquid from the interior in the direction of the arrows.[37]
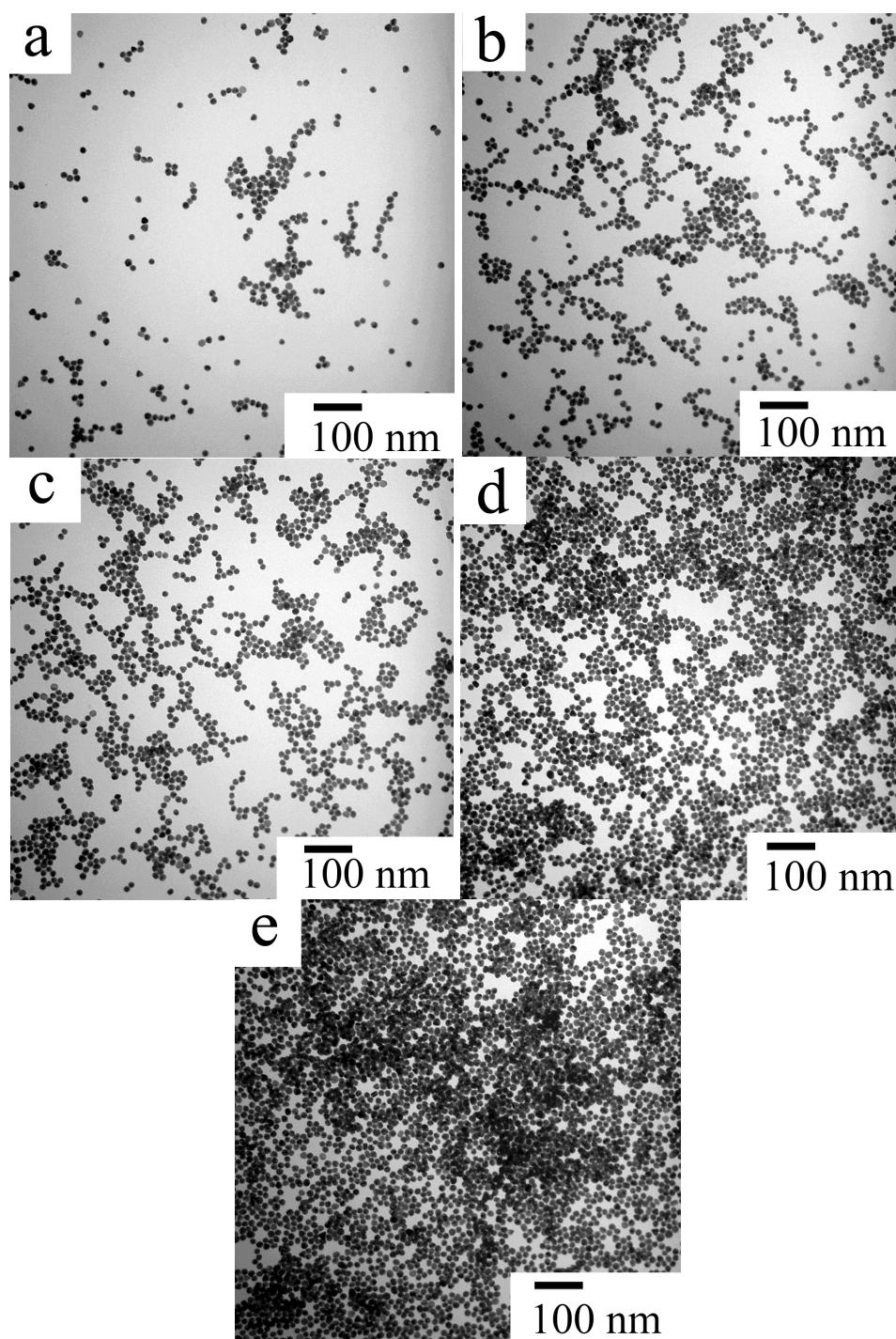
Figure 16: TEM images of self-assemblies of 4 μL of 15 nm Au NP-PVOH conjugates: (a) 6x; (b) 24x; (c) 42x; (d) 100x; and (e) 200x concentrated.

IV. Optimization of cast volume. We speculated that the amount of Au NP-PVOH drop cast should be reduced to minimize aggregation and 3D self-assemblies, thus enhancing 2D self-assemblies. Overall, decreasing the volume of the drop allows for shorter evaporation time so that the resulting film should have minimized coffee ring effect and a more uniform distribution of Au NPs. The casted volume of Au NP-PVOH solution was decreased from 4 μL to 2 μL. The following concentrations were studied after adjusting the cast volume: 100x, 200x, and 400x. By decreasing the volume of the amount of Au NP-PVOH cast, a uniform distribution of Au NPs was observed on the grid at a lower magnification. In the 100x sample, the Au NPs were arranged in a monolayer, but the Au NPs were sparse and not close enough to each other (Figure 17a). In the 200x and 400x samples, the Au NPs were very close to one another, and 2D self-assembly was observed (Figure 17b and c). At 400x, the short interparticle distance, due to the increase in Au NP concentration, promoted 2D self-assemblies. Although there were some 3D self-assemblies, we optimized our concentration at 400x with 2μL cast volume.
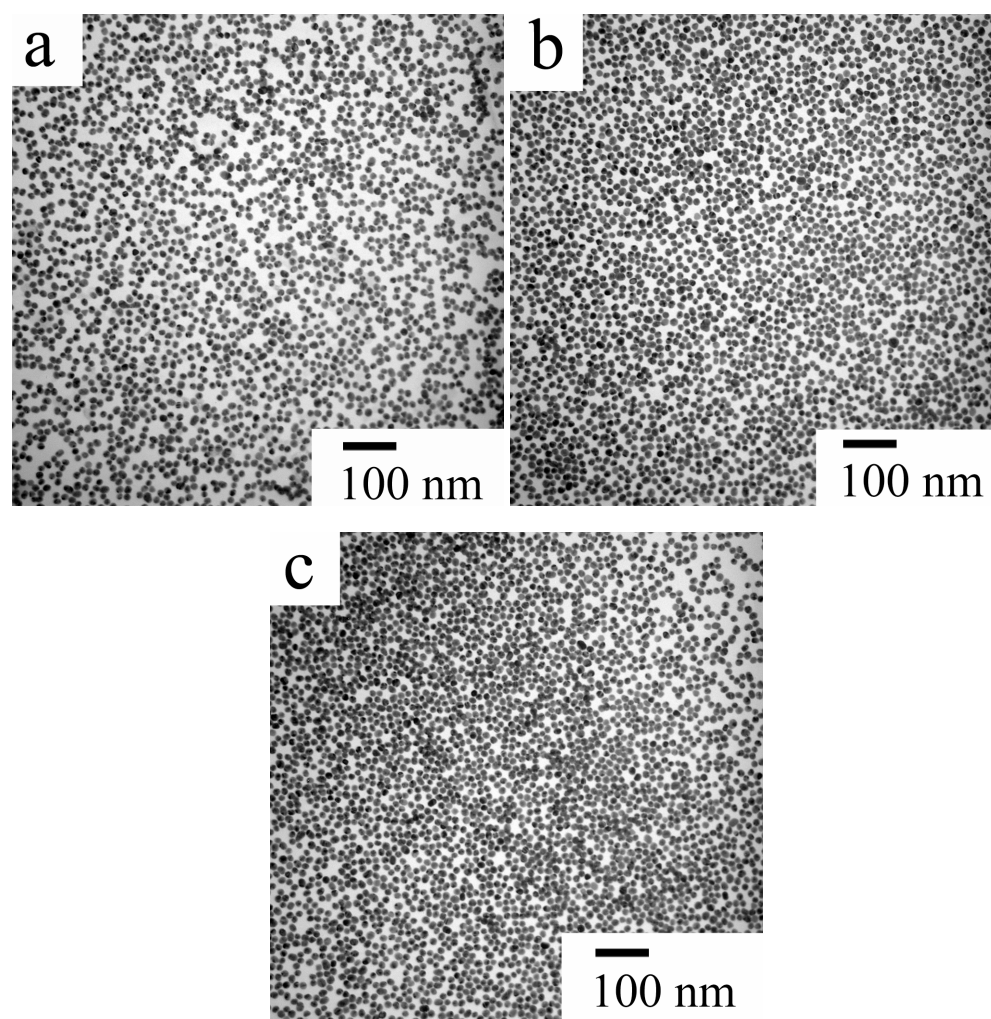
Figure 17: Self-assemblies of 15 nm Au NP-PVOH conjugates cast from 2 μL solution at concentrations of (a) 100x; (b) 200x; and (c) 400x of the original.

A few of the challenges in working with aqueous solution are phase segregation and void formation.[20] Due to the slow evaporation of water, when a drop of Au NP-PVOH solution is allowed to dry at room temperature on a TEM grid, smaller water droplets can separate from the Au NP-PVOH solution. When the droplets dry, they leave behind voids (Figure18a), which exclude Au NP-PVOH from those regions. Additionally, the slow water

evaporation can result in phase segregation (Figure 18b) into particle poor and particle rich regions. Both of these factors interfere with 2D self-assembly.
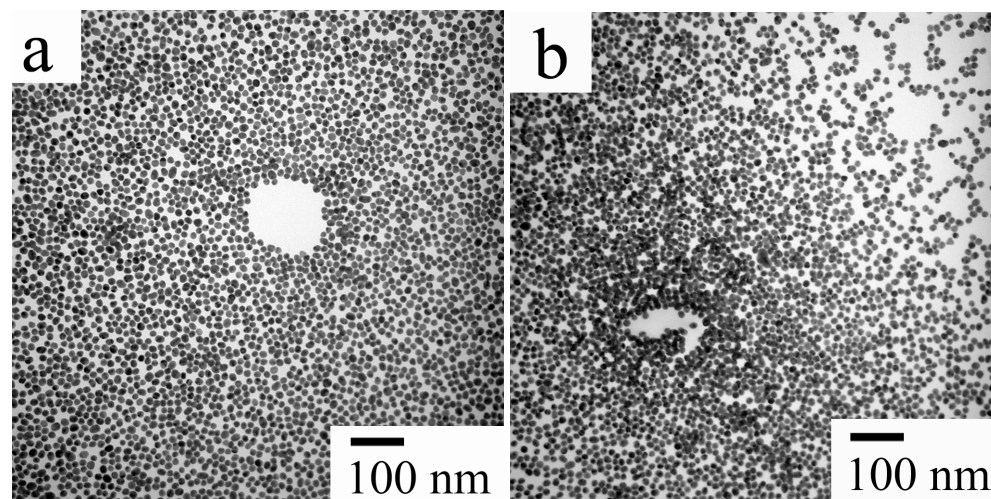
Figure 18: Issues of (a) void formation; and (b) phase segregation due to slow evaporation of water.

V. Heat Treatment. The second factor that could promote 2D self-assemblies is heat treatment. Using 400x concentration, in order to eliminate the issues associated with the slow evaporation of water, heat treatment was introduced to accelerate the evaporation of water, thus reducing the issues of phase segregation and void formation. Initially, a dried film of 400x sample was heated at 110 ^{o}C for one hour under constant nitrogen flow. The temperature was selected to be above the glass transition temperature ($T_g = 85$ ^{o}C) and below the melting temperature ($T_m = 230\text{-}260$ ^{o}C)[18] of PVOH. Constant nitrogen flow was included to prevent the oxidation of PVOH at high temperature. Ideally heat treatment at an optimal temperature for an optimal amount of time would break the strong hydrogen bonds

between the hydroxyl groups in PVOH in order to promote PVOH chain mobility. Mobility would allow rearrangement of the positions of the Au NP-PVOH conjugates to eliminate particle poor and particle rich regions as well as to fill in the circular voids. However, voids and phase segregation remained throughout the film as well as 2D and 3D self-assemblies in some regions (Figure 19). We suspected that since the film was air-dried before the heat treatment, the PVOH chains were unable to move sufficiently away from their original locations even at a high temperature.

ervig4
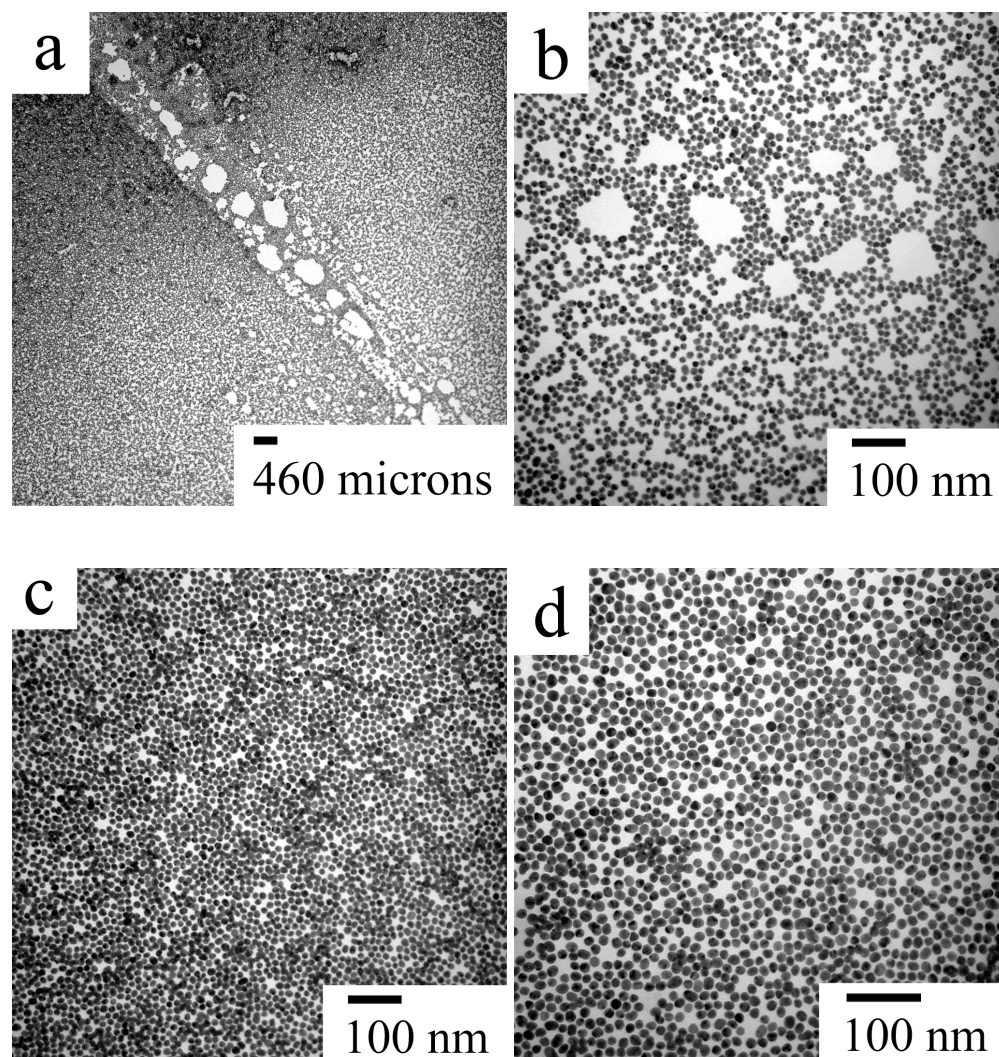
Figure 19: Self-assembly of air-dried film of Au NP-PVOH conjugates after heating at 110 °C for 1 h. (a, b) Voids were present throughout the film; (c) 3D and (d) 2D self-assemblies.

In order to test our hypothesis that heat treatment improves 2D self-assembly by accelerating the drying process and providing PVOH chain mobility, we cast a 2 μL drop of Au NP-PVOH solution on a TEM grid, and immediately heated the sample at 110 °C for one hour under nitrogen. Referring to Figure 20a, which is the overview of the TEM grid, each square

mesh within the grid has a similar pattern of Au NP distribution as indicated by the ripples of dark lines. This indicated that the coffee ring effect was significantly reduced due to the heat treatment. Within each square mesh, the Au NP-PVOH self-assembly resembled that in Figure 20b and c. Since the coffee ring effect was reduced, it appeared as if the film was darker or more concentrated compared to the film in Figure 17c. However, this effect could be accounted for by the uniform distribution of the Au NPs from the center to the edge of the film instead of all the Au NPs being concentrated at the edge of the film. As a result of uniform distribution, 3D self-assemblies predominated throughout the film. Many aggregates of Au NPs were seen and few, if any, 2D self-assemblies were observed.
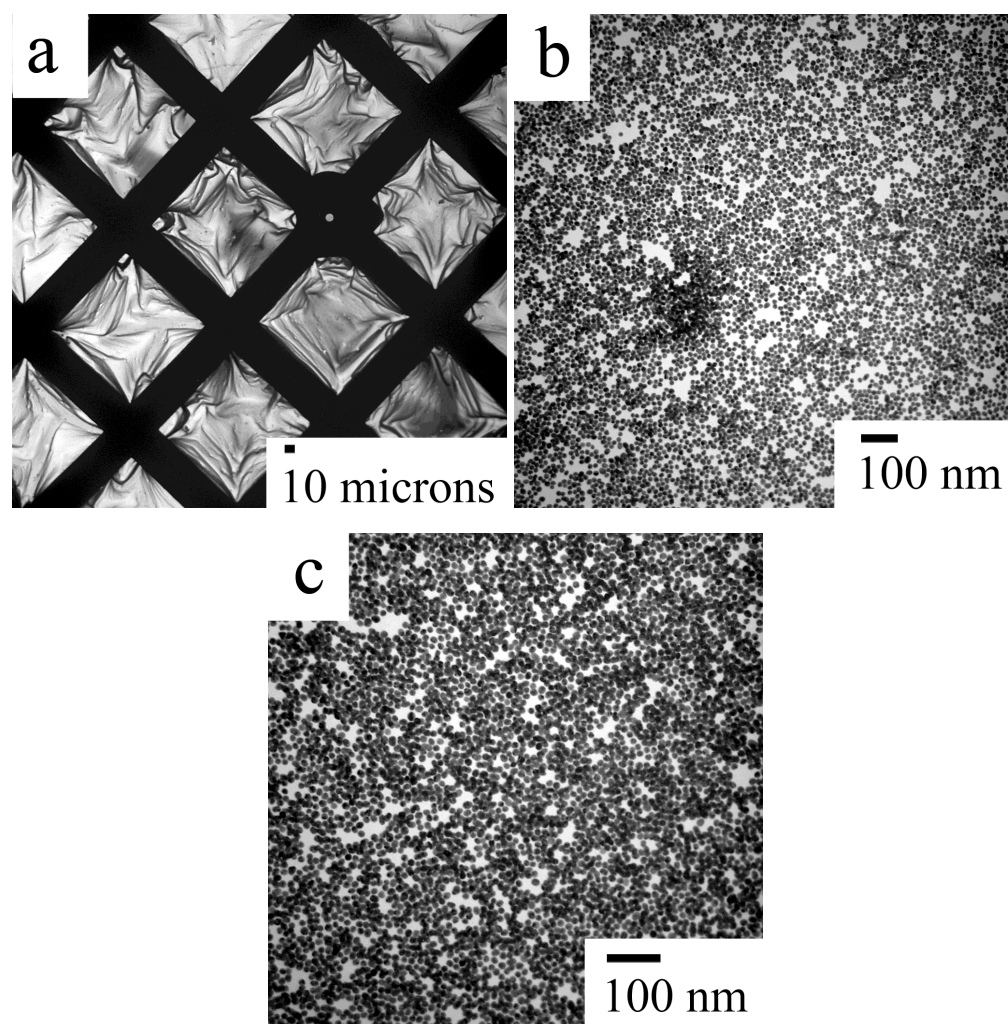
Figure 20: AuNP-PVOH conjugates (400x concentrated) dried immediately at 110 ^{o}C for one hour: (a) overview of the Au NP-PVOH film at a low magnification; (b) 2D; and (c) 3D self-assemblies.

Looking closer at the 3D self-assembly in Figure 20c, a monolayer of 2D self-assemblies is present underneath a partial second layer of Au NPs. Thus, in order to achieve just 2D self-assembly, the concentration was decreased to eliminate the 3D self-assembly or the excess Au NPs that deposited on top of the monolayer. The Au NP concentration was reduced

from 400x to 200x and 2D self-assemblies were observed (Figure 21c and d).

In the overview of the grid (Figure 21a), there was no prominent pattern of

ripple formation as a result of the drying process and lower Au NP

concentration. Because we cannot completely escape the evaporation

mechanism of water, there were fewer Au NPs in the center of the film than in

the regions towards the perimeter of the film. This phenomenon can be seen as

a gradient in Au NP concentration in Figure 21b. However, the majority of the

square mesh displayed 2D self-assemblies away from the center of the film as
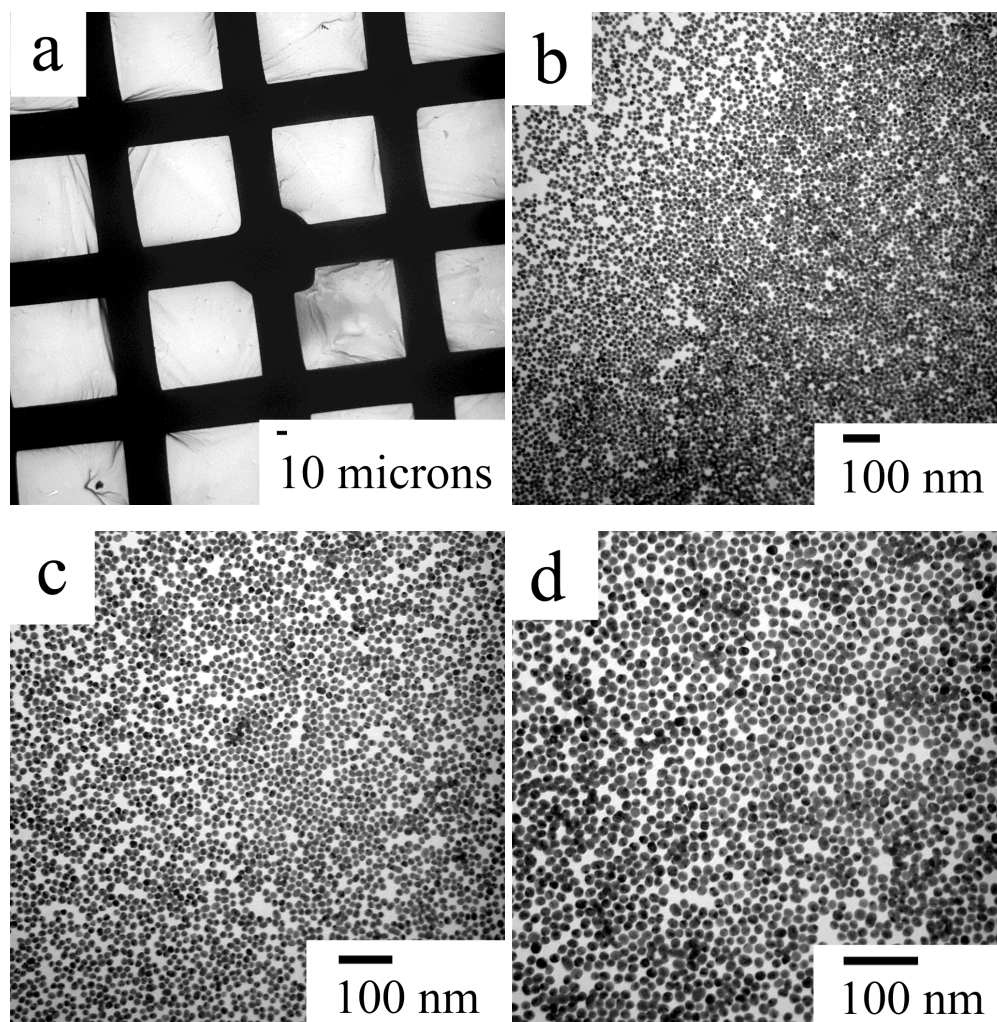
indicated in Figure 21c and d.

Figure 21: Au NP-PVOH conjugates (200x concentrated) dried immediately at 110 $^{\circ}$C for one hour: (a) no prominent ripples were seen at a low magnification of the grid; (b) 2D and 3D self-assemblies; (c, d) the majority of the grid had 2D self-assemblies.

After achieving ordered 2D self-assemblies in the Au NP-PVOH films post one-hour heat treatment, we were interested in whether extended heating time would promote the ordering process further, thus we increased the heating time to two hours. As seen in Figure 22b, the center of the film had more Au NP poor regions than on the film after one-hour heat treatment. However, towards the outer regions of the film, some 2D self-assemblies were observed (Figure 22c and d). Overall the two-hour heat-treated sample was not as ordered as the one after one-hour heat treatment. We concluded that although 2D self-assemblies were also seen in the 2-hour heat-treated sample, increased heating time did not necessarily improve 2D self-assembly. Thus, we optimized our heating time to be one hour.
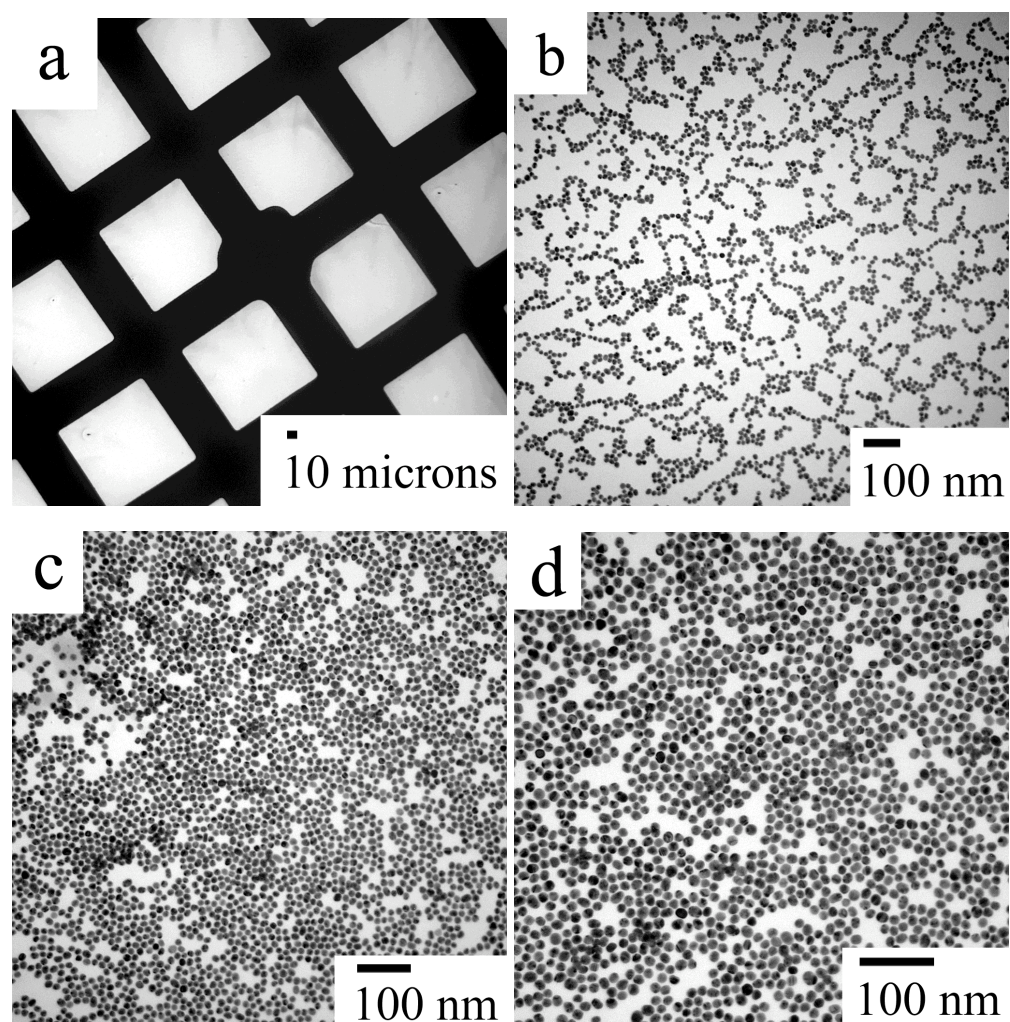
Figure 22: Self-assembly of Au NP-PVOH conjugates after a two-hour heat treatment: (a) overview of the film; (b) particle poor regions in the center of the film; (c,d) 2D self-assemblies.

IV. PVOH degree of hydrolysis. The third factor that may affect 2D self-assemblies is PVOH degree of hydrolysis. The unhydrolyzed portion is poly(vinyl acetate) (PVAc), which is the precursor to PVOH. The acetate group in PVAc is thought to provide "softness" to the polymer by weakening the hydrogen bonding between the hydroxyl groups of PVOH.[18] The "softness" factor is hypothesized to promote increased mobility of the chains by decreasing the crystallinity of the film. Thus, we extended our study to include two other PVOH chains of comparable molecular weights to 13-23 kDa, but different degrees of hydrolysis ranging from 98%, 88% to 80%. Ordered monolayers and 2D self-assemblies in all three types of PVOH samples were achieved. There were some 3D self-assemblies and voids in a few regions of the grid. However, as shown in Figure 23, majority of the Au NPs were evenly distributed throughout the films and no significant aggregates were observed. Additionally, although the degree of hydrolysis was different in all three PVOH samples, there were no significant differences among the self-assemblies.

After achieving ordered, 2D self-assemblies of Au NP-PVOH conjugates, using ImageJ, the average adsorbed PVOH thickness of the three types PVOH samples in the crystalline state (post heat-treatment) was calculated to be roughly 0.8 nm. Compared to the hydrodynamic adsorbed PVOH thickness ($D_{H, PVOH\ thickness}$) of about 9.71 nm, the adsorbed layer in the crystalline state is exceedingly thinner.

In order to assess if 0.8 nm is a reasonable thickness, it was compared to the expected adsorbed thickness (in appendix) of 3.2 nm, which assumed that the dried PVOH chain remains spherical. The discrepancy between the expected thickness of 3.2 nm and experimental thickness of 0.8 nm can be explained by two hypotheses. 1) It could be that the size and most likely the conformation of the adsorbed PVOH chains reduced dramatically once the water molecules evaporated. Therefore, assuming that each PVOH chain that adsorbed to the Au NP surface was not close-packed, the dehydrated PVOH chains may have spread or flattened on the Au NP upon drying. 2) Due to centrifugation, the adsorbed PVOH chains were spun off from the Au NP surface.
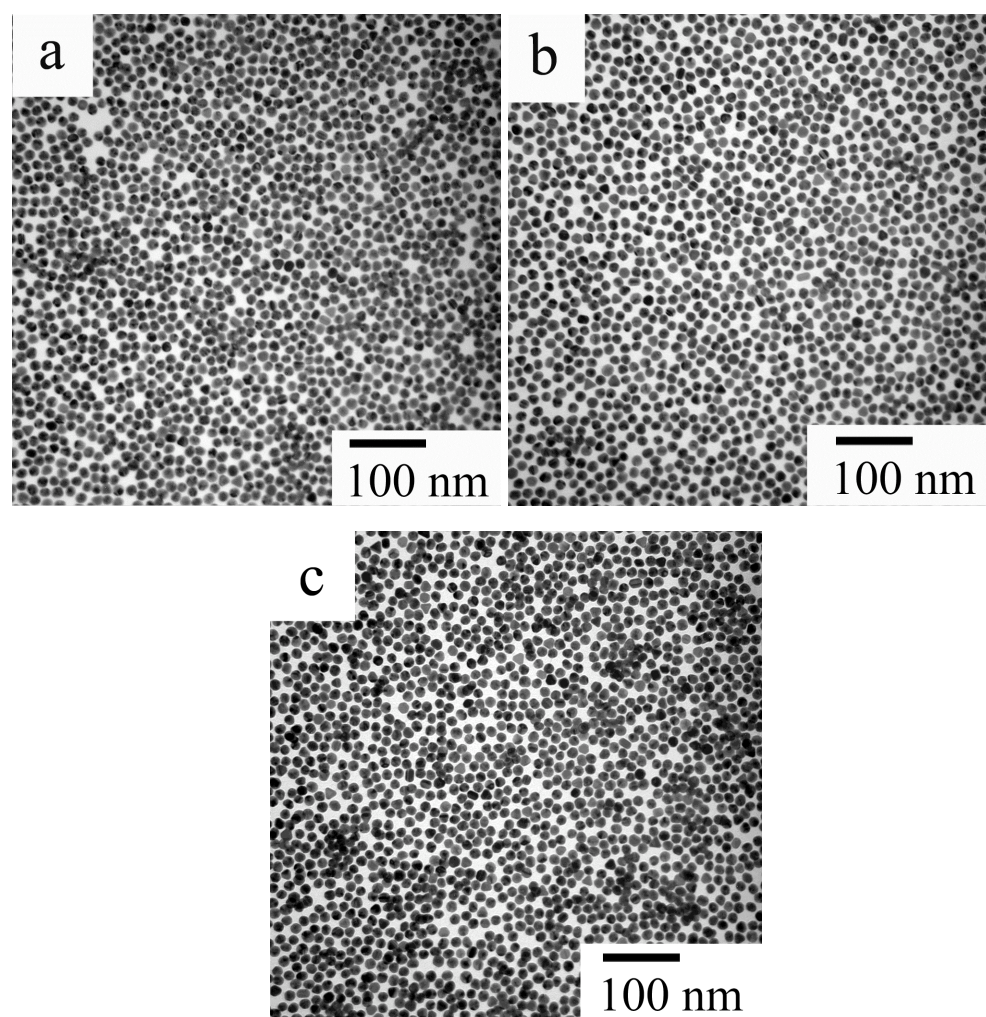
Figure 23: Ordered two-dimensional self-assemblies of Au NPs in PVOH films of comparable molecular weights, but differing degrees of hydrolysis: (a) 98%; (b) 88%; and (c) 80%.

CONCLUSIONS

Ordered two-dimensional self-assemblies of 15 nm Au NP-PVOH conjugates, of comparable molecular weights and varying degrees of hydrolysis of PVOH polymers, in the solid state were achieved from their aqueous solutions. No significant differences in 2D self-assemblies were observed among the three types of Au NP-PVOH conjugates.

The factors affecting 2D self-assemblies were studied and optimized in this research. First, 13-23 kDa and 98% hydrolyzed PVOH was chosen and Au NP-PVOH concentration was optimized at 200x and the volume of Au NP-PVOH solution cast was 2 μL. After optimizing the concentration, localized regions of 2D self-assemblies were observed under TEM. However, there were disordered regions due to phase segregation and void formation during the slow evaporation of water. In order to address those issues, heat treatment, which was the second factor studied, was introduced to accelerate drying and to increase the polymer chain mobility. Heat treatment was carried out at 110 $^{\circ}$C for one hour under nitrogen flow. Issues of aggregation, phase segregation, and void formation were reduced, and order in the 2D self-assembly was enhanced. The third factor examined was whether decreasing the degree of PVOH hydrolysis would further improve order in self-assemblies. Ordered 2D self-assemblies were observed in all three types of conjugates with PVOH polymers of comparable molecular weights and

different degrees of hydrolysis (98%, 88%, and 80%). However, improvement

in the 2D self-assembly was not obvious at lower degrees of hydrolyzed

PVOH samples.

FUTURE WORK

This project has examined three out of six factors affecting 2D self-assembly of Au NP-PVOH conjugates in the solid state from their aqueous solutions. For future work, there are three main areas remaining to be investigated. First, as an extension of this project, optimization of heat treatment in terms of temperature and time (to allow PVOH chain mobility without causing degradation and oxidation) will be explored. Furthermore, the effect of PVOH molecular weight, which would affect interparticle spacing, and the effect of Au NP size and shape on 2D self-assembly will be examined. Achieving hexagonally close-packed Au NPs in PVOH matrices is the ultimate goal after optimizing all of the parameters as it has not been previously accomplished using PVOH or an aqueous system.

When PVOH chains (that are adsorbed to Au NPs) of varying degrees of hydrolysis are heated, heating temperature and time may need to be customized for each PVOH. The variation in the degree of hydrolysis changes polymer composition, i.e. the relative amounts of PVOH and PVAc. The former is a crystalline (hard) and the latter is an amorphous (soft) polymer, thus heat treatment conditions need to be tailored toward achieving polymer mobility, which is likely composition dependent.

The starting PVOH molecular weight of this project was selected to be 13-23 kDa based on a previous study involving Au NP- polystyrene

conjugates; 13 kDa was the upper limit in order to achieve hexagonal 2D self-assemblies. However, this project thus far revealed that 13-23 kDa may be the lower limit since the interparticle spacing between the Au NPs in Figure 3 is much wider than the interparticle spacing in Figure 23. The much reduced interparticle spacing in the PVOH system is an indication of much "flatter" conformation of adsorbed PVOH compared to the end-attached polystyrene, which is likely to be more extended away from NPs. The molecular weight of PVOH controls the interparticle spacing or distance between neighboring Au NPs in thin films. Therefore, the molecular weight should be increased in order to achieve improvements in (hexagonal) 2D self-assembly.

Lastly, given time and resources, after optimizing all the conditions to achieve hexagonal 2D self-assemblies using spherical Au NPs of different sizes, the study can be extended to include different Au NP shapes to also achieve 2D self-assembly. As mentioned in the introduction, different Au NP sizes absorb slightly different wavelengths of light. Also, when the shape of Au NPs is changed, e.g. spherical to rodlike, the absorption splits into two bands. Thus, depending on the application, a preference towards one absorption maximum can be accomplished by simply changing the NP size or shape.

REFERENCES

(1) Link, S.; El-Sayed, M. A. *J. Phys. Chem. B.* **1999***, 103*, 8410-8426.

(2) Seoudi, R. *Physica B.* **2008***, 403*, 4236-4240.

(3) Daniel, M. C.; Astruc, D. *Chem. Rev.* **2004***, 104*, 293-346.

(4) El-Sayed, I.; Xiaohua, H.; El-Sayed, M. A. *Nano Lett.* **2005***, 5*, 829-834.

(5) El-Brolossy, T. A.; Abdallah, T.; Mohamed, M. B.; Abdallah, S.; Easawi, K.; Negm, S.; Talaat, H. *Eur. Phys. J. Special Topics* **2008***, 153*, 361-364.

(6) Papavassiliou, G. C. *Prog. Solid State Chem.* **1980***, 12*, 185.

(7) Lee, Z.; Jeon, K.; Dato, A.; Erni, R.; Richardson, T. J.; Frenklach, M.; Radmilovic, V. *Nano Lett.* **2009***, 9*, 3365-3369.

(8) Kumar, S.; Gandhi, K. S.; Kumar, R. *Ind. Eng. Chem. Res.* **2007***, 46*, 3128-3136.

(9) Basu, S.; Pande, S.; Jana, S.; Bolisetty, S.; Pal, T. *Langmuir* **2008***, 24*, 5562-5568.

(10) Yockell-Lelièvre, H.; Desbiens, J.; Ritcey, A. M. *Langmuir* **2007***, 23*, 2843-2850.

(11) Rechberger, W.; Hohenau, A.; Leitner, A.; Krenn, J. R.; Lamprecht, B.; Aussenegg, F. R. *Opt. Commun.* **2003***, 220*, 137-141.

(12) Roca, M.; Pandya, N. H.; Nath, S.; Haes, A. J. *Langmuir* **2009***, 26*, 2035-2041.

(13) Tang, X.; Jiang, P.; Ge, G.; Tsuji, M.; Xie, S.; Guo, Y. *Langmuir* **2008***, 24*, 1763-1768.

(14) Porel, S.; Singh, S.; Harsha, S. S.; Rao, D. N.; Radhakrishnan, T. P. *Chem. Mater.* **2005***, 17*, 9-12.

(15) Van der Zande, B.; Pages, L.; Hikmet, R. A. M.; van Blaaderen, A. *J. Phys. Chem. B.* **1999***, 103*, 5761-5767.

(16) Khanna, P. K.; Gokhale, R.; Subbarao, V. V. V. S.; Kasi Vishwanath, A.; Das, B. K.; Satyanarayana, C. V. V. *Mat. Chem. Phys.* **2005***, 92*, 229-233.

(17) Lin, H. L.; Liu, Y. F.; Yu, T. L.; Liu, W. H.; Rwei, S. P. *Polymer* **2005***, 46*, 5541-5549.

(18) Mark, H. F.; Kroschwitz, J. I. In *Encyclopedia of Polymer Science and Technology;* Wiley-Interscience: New York, 1985; .

(19) Tester, C. C. Dynamic Light Scattering Studies of the Interaction Between Gold Nanoparticles and Poly(vinyl alcohol), Mount Holyoke College, 2007.

(20) Zhao, S.; Wang, S.; Kimura, K. *Langmuir* **2004***, 20*, 1977-1979.

(21) Gao, F.; Lu, Q.; Komarneni, S. *Chem. Mater.* **2005***, 17*, 856-860.

(22) Harfenist, S. A.; Wang, Z. L.; Whetten, R. L.; Vezmar, I.; Alvarez, M. M. *Adv. Mater.* **1997***, 9*, 817-822.

(23) Stoeva, S.; Klabunde, K. L.; Sorensen, C. M.; Dragieva, I. *J. Am. Chem. Soc* **2003***, 12*, 2305-2311.

(24) He, S.; Yao, J.; Jiang, P.; Shi, D.; Zhang, H.; Xie, S.; Pang, S.; Gao, H. *Langmuir* **2001***, 17*, 1571-1575.

(25) Brown, L. O.; Hutchison, J. E. *J. Phys. Chem. B.* **2001***, 105*, 8911-8916.

(26) Giersig, M.; Mulvaney, P. *Langmuir* **1993***, 9*, 3408-3413.

(27) Abe, K.; Hanada, T.; Yoshida, Y.; Tanigaki, N.; Takiguchi, H.; Hagasawa, H.; Nakamoto, M.; Yamaguchi, T.; Yase, K. *Thin Solid Films* **1998***, 327-329*, 524-527.

(28) Huang, S.; Tsutsui, G.; Sakaue, H.; Shingubara, S.; Takahagi, T. *Jpn. J. Appl. Phys. Part 2: Lett.* **1999***, 38*, L473.

(29) Wu, C. K.; Hultman, K. L.; O'Brien, S.; Koberstein, J. T. *J. Am. Chem. Soc. ,* **2008***, 130*, 3516-3520.

(30) Teranishi, T.; Hasegawa, S.; Shimizu, T.; Miyake, M. *Adv. Mater.* **2001***, 13*, 1699-1701.

(31) Srivastava, S.; Frankamp, B. L.; Rotello, V. M. *Chem. Mater.* **2005***, 17*, 487-490.

(32) Rutgers, A. J.; Nagels, P. *Nature* **1953***, 171*, 568.

(33) Bozzola, J. J.; Russell, L. D. In *Electron Microscopy;* Jones and Bartlett: Sudbury, 1999; Vol. 2nd ed., pp 470.

(34) The Transmission Electron Microscope.

    http://nobelprize.org/educational_games/physics/microscopes/tem/index.
    html (accessed 02/20, 2010).

(35) Zetasizer Nano Series User Manual.
    http://www.nbtc.cornell.edu/facilities/downloads/Zetasizer%20Manual.pd
    f (accessed 02/20, 2010).

(36) Dynamic Light Scattering: An Introduction in 30 Minutes
    http://www.malvern.com/common/downloads/campaign/MRK656-01.pdf
    (accessed 02/20, 2010).

(37) Why do drying drops form a ring?
    http://mrsec.uchicago.edu/research/nuggets/coffee/.

APPENDIX

To determine the expected size (d) of dehydrated PVOH chains:

9.71 nm
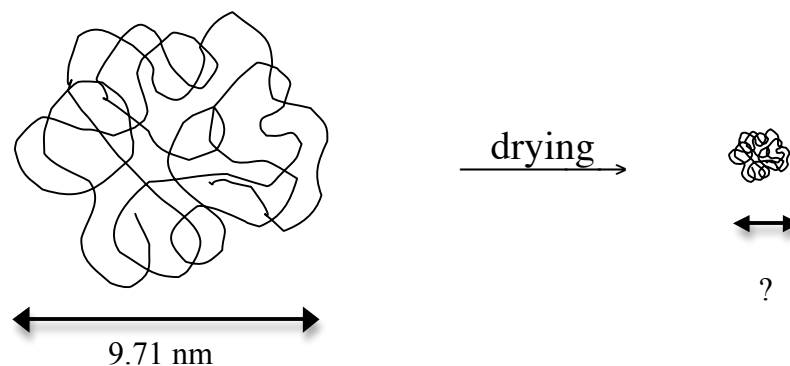
Assume the dried PVOH chain of 13,000 g/mol of 1.2 g/cm^3 remains spherical (PVOH film density: 1.19 – 1.31 g/cm^3):

$$13{,}000\,\frac{g}{mol}\times\frac{1\ mol}{6.022\times10^{23}}\times\frac{1\ cm^3}{1.2\ g}\times\frac{(10^7\ nm)^3}{(1\ cm)^3}\;=\;\frac{4}{3}\pi(\frac{d}{2})^3$$

$$17.99\ nm^3\;=\;\frac{1}{6}\pi\,d^3$$

$$d\;=\;3.2\ nm$$